Preprints.org

Article

The Impact of Bilirubin on 7α- and 7β-Hydroxysteroid Dehydrogenases: Spectra and Docking Analysis

Qingzhi Ji [*] , Jiamin Chen , Luping Zhu , Ruiyao Wang , Bochu Wang

Article

The Impact of Bilirubin on 7α- and 7β-Hydroxysteroid Dehydrogenases: Spectra and Docking Analysis

Qingzhi Ji [1,*], Jiamin Chen [1], Luping Zhu [1], Ruiyao Wang [1] and Bochu Wang [2]

[1]   Jiangsu Province Engineering Research Center of Tumor Targeted Nano Diagnostic and Therapeutic Materials, School of Pharmacy, Yancheng Teachers University, Yancheng, Jiangsu 224007, P. R. China.

[2]   College of Bioengineering, Chongqing University, Chongqing 400030, P. R. China.

*   Correspondence: jiqingzhi202@126.com; Tel.: +86-0515-88258773

Abstract: 7α- and 7β-hydroxysteroid dehydrogenases (HSDH) are a pair of enzymes that can catalyze the isomerization of hydroxyl group at site 7 of bile acids. In previous study, we found that the activities of 7α- and 7β-HSDH can be inhibited by bilirubin. In order to clarify the impact, the effects of bilirubin on enzymes were studied by kinetics, spectrum and docking analysis. Relative activity of 7α-HSDH remained less than 40 % under 1 mM bilirubin, for 7β-HSDH, only 18 % activity left at the same condition. Using taurochenodeoxycholic acid (TCDCA) as substrate, the K_m of 7α-HSDH was up to 0.63 mM from 0.24 mM after binding with bilirubin, the K_m of 7β-HSDH rose from 1.14 mM to 1.87 mM for the catalysis of tauroursodeoxycholic acid (TUDCA). The affinity of 7α- and 7β-HSDH to substrate decreased with the effect of bilirubin. The binding of bilirubin with 7α- or 7β-HSDH were analyzed by UV–Vis spectra, Fluorescence spectra and Circular dichroism (CD) spectra. The results reflected that bilirubin caused a slight change in the secondary structure of 7α- or 7β-HSDH, and the changes were correlated with the ratio of bilirubin to enzyme. 10 candidate molecular docking results were presented to reflect the binding of bilirubin with 7α- or 7β-HSDH and to explore the inhibition mechanism. This research not only provides the more in-depth understanding of 7α- and 7β-HSDH, but also reminds us to avoid the inhibition of bilirubin on hydroxysteroid dehydrogenases.

Keywords: bilirubin; 7α- and 7β-hydroxysteroid dehydrogenases; activity; inhibition

1. Introduction

Bile acids are mainly synthesized in the liver from cholesterol, stored in the gallbladder, and metabolized in the intestine by the gut microbiota [1,2]. The specific bile acids can activate important nuclear receptors, farnesoid X receptor (FXR) and one G protein-coupled receptor (TGR5). Microbial modifications of bile acids influence the host metabolism *via* the bile acid receptors FXR and TGR5, which suggest that such agonists may prove useful in the treatment of many diseases [2]. Among the bile acids, ursodeoxycholic acid (UDCA) and its conjugated form Tauroursodeoxycholic acid (TUDCA) are the ones with highest medicinal value. UDCA is the only drug for the treatment of primary biliary cirrhosis (PBC) approved by FDA so far. UDCA have been effectively used to treat hepatobiliary disease by relieving hepatic steatosis and reducing liver fibrosis [3–5]. UDCA and TUDCA can prevent vision and hearing loss, can slow retinal degeneration [6,7]. Due to the function of blood–brain barrier crossing, UDCA and TUDCA exert effects on the central nervous system, especially in Alzheimer's disease (AD) and Parkinson's disease therapies [8,9]. Furthermore, TUDCA also can promote vascular repair [10], inhibit obesity [11,12] and enhance islet function [13]. Especially, the paper published in November 2022 attracted people's attention, which reported that the down regulation of ACE2 mediated by UDCA can reduce susceptibility to SARS-CoV-2 [14].

According to previous studies, chenodeoxycholic acid (CDCA) and its conjugated form taurochenodeoxycholic acid (TCDCA), could be directly transformed into UDCA or TUDCA in vitro

with the catalysis of 7α- and 7β- hydroxysteroid dehydrogenases (HSDH) [15,16], as Figure 1a. Relying on the circulation of nicotinamide adenine dinucleotide phosphate (NADP$^+$ and NADPH), the two steps coupling-reaction is highly efficient in preparation of UDCA and TUDCA. 7α- and 7β-HSDH belong to short chain dehydrogenase/reductase (SDR) family, which have been discovered from series of gut microbes, such as *Clostridium absonum* [17], *Bacteroides fragilis* [18], and *Xanthomonas maltophilia* [19], *Candidatus Ligilactobacillus* [20]. Besides, there are some progresses of 7α- and 7β-HSDH in application. 7α- and 7β-HSDH have been successfully expressed in *E. coli* and purified using specific tags [17,21]. Furthermore, both free enzymes and immobilized enzymes are suitable for the two steps catalytic reactions. Besides, the waste chicken bile is rich in TCDCA, the sufficient source of substrate can be ensured [22]. Bilirubin is one of the main components of waste chicken bile, from which substrate TCDCA is obtained. In summary, this strategy affords an efficient and clean process for production of TUDCA.

Bilirubin is a yellow compound that occurs in the normal catabolic pathway, known for its antioxidant properties. Bilirubin is synthesized by the activity of biliverdin reductase on biliverdin. Both bilirubin and biliverdin are the products of heme catabolism. Bilirubin, when oxidized, reverts back to biliverdin once again [23,24]. Recently, bilirubin has been recognized as a hormone with endocrine actions. Current studies also show that bilirubin can decrease adiposity and prevent metabolic and cardiovascular diseases [25]. Bilirubin can act as an agonist activate the (melastatin-like transient receptor potential 2) TRPM2 channel to exacerbate neurotoxicity [26].The structure of bilirubin was presented in Figure 1b.
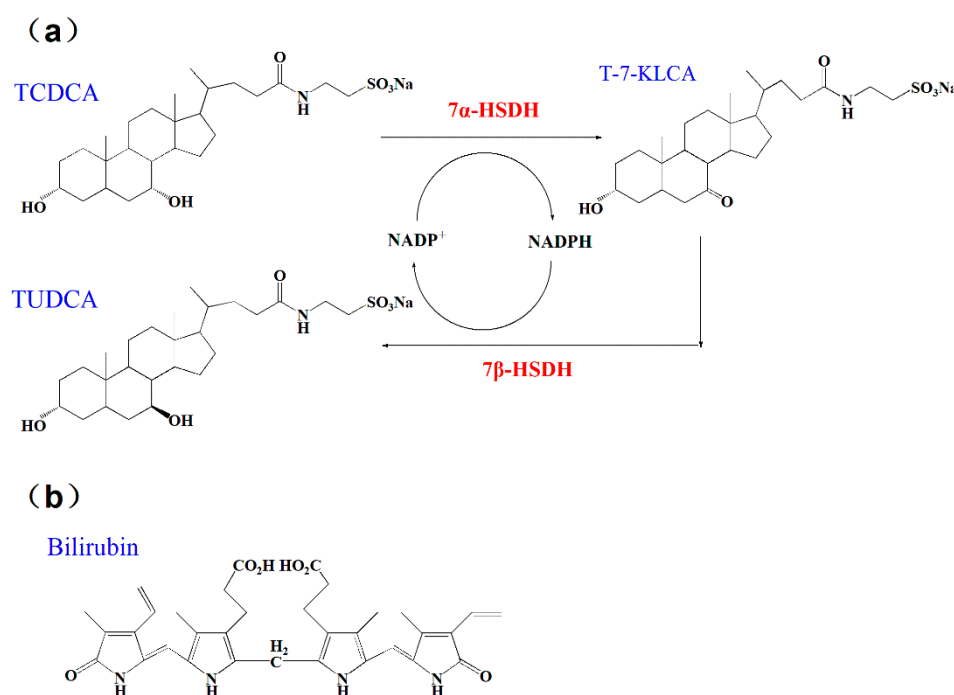

Figure 1. (**a**) The transformation of TCDCA to TUDCA with the catalysis of 7α- and 7β-HSDH. NADP$^+$ and NADPH used as cofactors; (**b**) The structure of bilirubin.

The combination of substances can be achieved in a variety of ways such as self-assembly [27,28], co-precipitation [29,30] and immobilization [31,32]. The combination of bilirubin to albumin can proceed spontaneously and the binding of bilirubin and albumin has long been explored by scientists, which possess a variety of physiological functions in human body [33–35]. Serum unbound bilirubin concentration can act as an ideal marker that reflects changes in bilirubin binding to albumin. Disorders of bilirubin binding to albumin may be associated with neurologic dysfunction [36]. The research also found that bilirubin binding capacity and affinity to albumin are low and variable in premature infants. Specific exogenous drugs, intravenous lipids, and a series of clinical factors may adversely affect bilirubin–albumin binding [37]. Arriaga et al. found that C1 esterase activity in

inhibited by unconjugated bilirubin [38]. Bilirubin showed a higher affinity for collagen at a concentration of about 25 nM/mg and the affinity rate for bilirubin to collagen has been found to be 8.89×10^{-3} s^{-1} [39]. Besides, the interaction between fibrinogen and bilirubin and the influence of bilirubin on the formation of fibrin and protection against oxidation, are described by Gligorijević et al. [40].

In previous study, we found that the activities of 7α- and 7β-HSDH affected by bilirubin. In particular, TUDCA yield decreased rapidly in the presence of bilirubin. It is meaningful to explore the impact of bilirubin on 7α- and 7β-HSDH, including the relative activity of enzymes, transformation rate of substrate, spectral changes of enzymes and possible inhibition mechanism. This research was focused on the impact of bilirubin on 7α- and 7β-HSDH. Firstly, the properties of 7α- and 7β-HSDH were studied after purification. Then, the effects of bilirubin on enzyme activity, kinetics and substrate transformation were carefully measured by UV absorption and High performance liquid chromatography (HPLC), respectively. In addition, the binding of bilirubin to 7α- or 7β-HSDH were analyzed by UV–Vis spectra, Fluorescence spectra and CD spectra. At last, molecular docking was used to present the binding conformation and explain the possible inhibition mechanism of bilirubin to enzymes.

2. Results and discussion

2.1. Properties of 7α- and 7β-HSDH

The target proteins, 7α- and 7β-HSDH, were successfully expressed in recombination *E. coli* and purified by GST Gene Fusion System in a mild condition without the process of denaturation by urea or guanidine hydrochloride. After purification and concentration, two enzymes were verified by SDS-PAGE as Figure 2a. According to standard protein marker, the molecular mass of 7α-HSDH is about 27 kDa, and 7β-HSDH is about 29 kDa. The results are nicely matching the previously sequenced 7α- and 7β-HSDH [17,18].
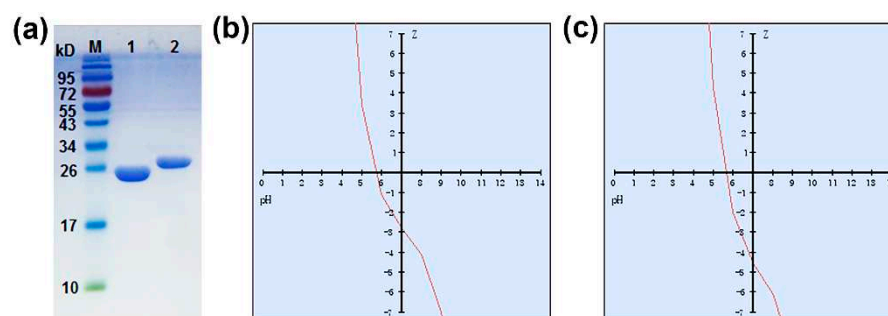

Figure 2. (**a**) Sodium dodecyl sulfate-polyacrylamide gel electrophoresis (SDS-PAGE) analysis of 7α- and 7β-HSDH. M: PageRuler pre-stained protein ladder, 10 to 170 kDa, Lane 1: 7α-HSDH, Lane 2: 7β-HSDH; (**b**) The variation of net charge for 7α-HSDH with pH; (**c**) The variation of net charge for 7β-HSDH with pH.

In addition, the peptide calculator was also used to explore the properties of 7α- and 7β-HSDH. The results were shown in Table 1. The variation of net charge with pH for 7α- and 7β-HSDH was described in Figure 2b, c. Both 7α- and 7β-HSDH are negatively charged at pH 7.0, -2.8 mV for 7α-HSDH and -4.6 mV for 7β-HSDH. The isoelectric points of 7α- and 7β-HSDH are 5.7 and 5.5, respectively. Two enzymes have the same ratio of hydrophilic residues (37%). Besides, the molecular weights estimated by peptide calculator (28289.16 g/mol for 7α-HSDH, 29382.85 g/mol for 7β-HSDH) were close to that determined by SDS-PAGE.

Table 1. The properties analysis of 7α- and 7β-HSDH.

	Molecular weight (g/mol)	Isoelectric point	Charge at pH =7.0	Average hydrophilicity	Ratio of hydrophilic residues
7α-HSDH	28289.16	5.7	-2.8	0.0	37 %
7β-HSDH	29382.85	5.5	-4.6	0.1	37 %

7α- and 7β-HSDH were cloned from *Clostridium absonum* ATCC27555，the Genbank number was JN191345. The properties of two enzymes were estimated by peptide calculator (Qiangyao, Shanghai).

2.2. The effects of bilirubin on enzymatic activity and kinetics

The effects of bilirubin on activities of 7α- and 7β-HSDH were studied by testing various bilirubin concentrations ranging from 0 to 1 mM in 50 mM Tris-HCl buffer (pH 8.5). Enzymatic activity without the effect of bilirubin was regarded as 100%, and the results were shown in Figure 3. With the increase of bilirubin, relative activity of two enzymes decreased sharply. The relative activity of 7α- HSDH remained less than 40 % in 1 mM bilirubin. What's more, the activity 7β-HSDH was more seriously affected by bilirubin compared with 7α-HSDH. For 7β-HSDH, only 18 % activity kept as the concentration of bilirubin was 1 mM in buffer. Due to different amino acid compositions and three-dimensional structures, there are differences in the maximum binding amount of bilirubin to 7α- or 7β-HSDH. Besides, the different activity of 7α- and 7β-HSDH at the same bilirubin concentration may be related to different inhibition mechanism.
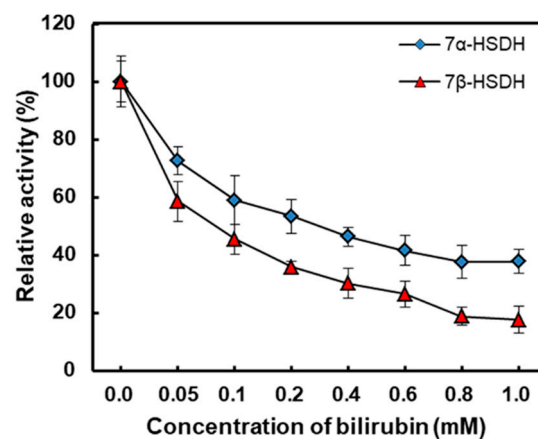

Figure 3. The effects of bilirubin on the activities of 7α- and 7β-HSDH. Enzymatic activity without the effect of bilirubin was regarded as 100%. Enzymatic activity was analysed at 25 °C in 50 mM Tris-HCl buffer (pH 8.5).

Kinetic constants of 7α-HSDH and 7β-HSDH were presented in Table 2. By measuring the reduction of NADP$^+$, we got a series of kinetic constants for 7α- and 7β-HSDH, such as V_{max}, K_m, k_{cat} and k_{cat}/K_m. K_m and V_{max} of free 7α-HSDH were 0.24 mM and 22.47 μmol/min using TCDCA as substrate. After binding with bilirubin, the K_m became 0.63 mM and V_{max} was as low as 6.78 μmol/min. k_{cat} changed from 6.25×10^3 s^{-1} to 1.02×10^3 s^{-1}. k_{cat}/K_m decreased from 2.60×10^4 s^{-1}· mM^{-1} to 1.62×10^3 s^{-1}· mM^{-1}. For cofactor NADP$^+$, the V_{max} of 7α-HSDH did not varied much, the K_m of 7α-HSDH rose to 0.59 mM from 0.28 mM with the effect of bilirubin. Similarly, after binding with bilirubin, V_{max} of 7β-HSDH for TUDCA decreased from 22.47 μmol/min to 4.32 μmol/min and K_m of 7β-HSDH for TUDCA rose from 1.14 mM to 1.87 mM. k_{cat} changed from 7.28×10^4 s^{-1} to 2.64×10^4 s^{-1}. k_{cat}/K_m decreased from 6.39×10^4 s^{-1}· mM^{-1} to 1.41×10^4 s^{-1}· mM^{-1}. For cofactor NADP$^+$, the V_{max} of 7β-HSDH varied from 53.61 μmol/min to 19.65 μmol/min, the K_m of 7β-HSDH only had a slight change from 1.37 mM to 1.32 mM with the effect of bilirubin.

After binding with bilirubin, the k_{cat} for both 7α-HSDH and 7β-HSDH reduced, and the catalysis rate of enzymes became slowly with the inhibition of bilirubin. So the results indicated that the

catalytic efficiency and the transformation ability seriously decreased after the enzymes bound with bilirubin. Furthermore, the affinity of 7α- and 7β-HSDH to substrate decreased after binding with bilirubin, which may be due to the change of their configuration. After immobilization on modified chitosan microsphere, the kinetic parameters of 7α- and 7β-HSDH changed similarly [16].

Table 2. The effect of bilirubin on kinetic constants of 7α- or 7β-HSDH.

Enzyme	Substrate	V_{max} ($\mu mol \cdot min^{-1} \cdot mg^{-1}$)	K_m (mM)	k_{cat} (s^{-1})	k_{cat}/K_m ($s^{-1} \cdot mM^{-1}$)
Free 7α-HSDH	TCDCA	22.47	0.24	6.25×10^3	2.60×10^4
	NADP$^+$	20.24	0.28	5.63×10^3	2.01×10^4
Free 7β-HSDH	TUDCA	52.80	1.14	7.28×10^4	6.39×10^4
	NADP$^+$	53.61	1.37	7.39×10^4	5.39×10^4
7α-HSDH+bilirubin	TCDCA	6.78	0.63	1.02×10^3	1.62×10^3
	NADP$^+$	18.76	0.59	2.82×10^3	4.78×10^3
7β-HSDH+bilirubin	TUDCA	4.32	1.87	2.64×10^4	1.41×10^4
	NADP$^+$	9.65	1.32	5.90×10^4	4.47×10^4

7α-HSDH+bilirubin and 7β-HSDH+bilirubin represented 7α-HSDH binding with 0.2 mM bilirubin and 7β-HSDH binding with 0.2 mM bilirubin, respectively.

2.3. The effect of bilirubin on enzymatic reaction

TCDCA can be transformed into TUDCA by the isomerisation of -OH at site 7 with the catalysis of 7α- and 7β-HSDH in two steps, as shown in Figure 1. The coupling-reaction has been reported [18,19]. In order to get accurate quantification of bile acids, the composition of reaction products was measured by High performance liquid chromatography with evaporative light-scattering detector (HPLC-ELSD). The peak positions of TCDCA (about 4.0 min), T-7-KLCA (about 4.6 min) and TUDCA (about 6.2 min) were presented in Figure 4.
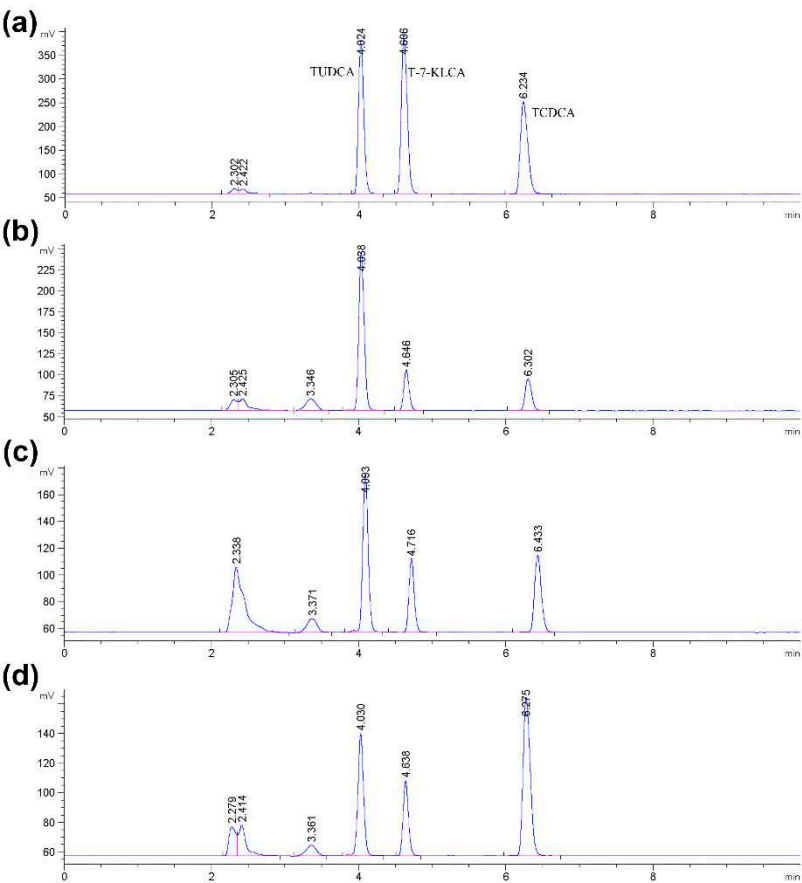
Figure 4. Bile acids in methanol were analyzed by HPLC-ELSD. (**a**) The concentration of the standard substance TCDCA was 0.5 mg/mL, and the injection volume was 10 μL; (**b**) TCDCA catalyzed by 7α- and 7β-HSDH without the inhibition of bilirubin; (**c**) TCDCA catalyzed by 7α- and 7β-HSDH with the inhibition of 0.2 mM bilirubin; (**d**) TCDCA catalyzed by 7α- and 7β-HSDH with the inhibition of 0.6 mM bilirubin.

Because of the inhibition of bilirubin on enzymes activity, the rate of catalysis would slow down, the substrate transformation and product yield would be less in a certain period of time. According to literature, acetone-derived extracts were more inhibitors for cellulase and decreased glucose yield for enzyme hydrolysis of Solka Floc (a lignin-free cellulose) by 42% [41]. Baksi et al. reported that the conversion of biomass to biofuel is substantiated with specific kinetics controlling enzymatic hydrolysis in presence of unavoidable inhibitors [42]. The results of TCDCA transformation in the absence or presence of bilirubin were shown in Figures 4 and 5. With the increase of bilirubin, both TCDCA conversion and TUDCA yield were gradually decreased. Without the inhibition of bilirubin on two enzymes, TCDCA conversion was more than 90%, and TUDCA yield was close to 60%. However, as the concentration of bilirubin was 0.8 mM in reaction buffer, TCDCA conversion remained 15% and TUDCA yield was only 5% in 4 hours. Furthermore, from the change of peak area, we can see that there was almost no conversion of TCDCA when the concentration of bilirubin in buffer was 0.8 mM. Except for bilirubin, the experiments showed that Cu^{2+} and Ca^{2+} also have some inhibition to 7α- and 7β-HSDH [22].
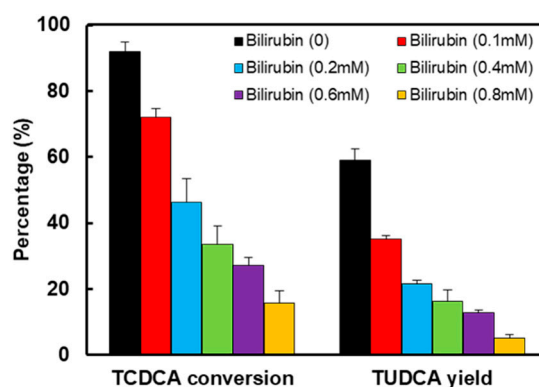

Figure 5. The effect of bilirubin on enzymatic reactions. The results were analysed by HPLC-ELSD. TCDCA conversion and TUDCA yield are expressed as the percentages of the substrate (TCDCA). The concentration of the substance TCDCA was 8mM, $NADP^+$ (2mM) as cofactor. The reaction time was 4 hours. The analyses were performed at 25 °C in 50 mM Tris-HCl buffer (pH 8.5).

2.4. Analysis of the binding of enzymes and bilirubin

To investigate the combination of bilirubin and enzymes, samples of 7α- or 7β-HSDH in the absence or presence of bilirubin were analysed by UV-Vis spectra, Fluorescence spectra and CD spectra, respectively.

At first, the combinations of bilirubin to 7α- or 7β-HSDH were analyzed by UV-Vis spectrum from 250 nm to 600 nm. The results were presented in Figure 6. There were not absorption peaks from 300 nm to 600 nm for free 7α- and 7β-HSDH. Bilirubin had an obvious absorption peak at about 438 nm, which was consistent with reference [43]. After binding to 7α- and 7β-HSDH, the main absorption became higher. Besides, upon binding to 7β-HSDH, the main absorption band of bilirubin was red shifted from 438 nm (bilirubin alone) to 442 nm. This result was similar to that have been reported. The main absorption band of bilirubin is shifted from 438 nm to 460 nm after binding to human serum albumin [43].
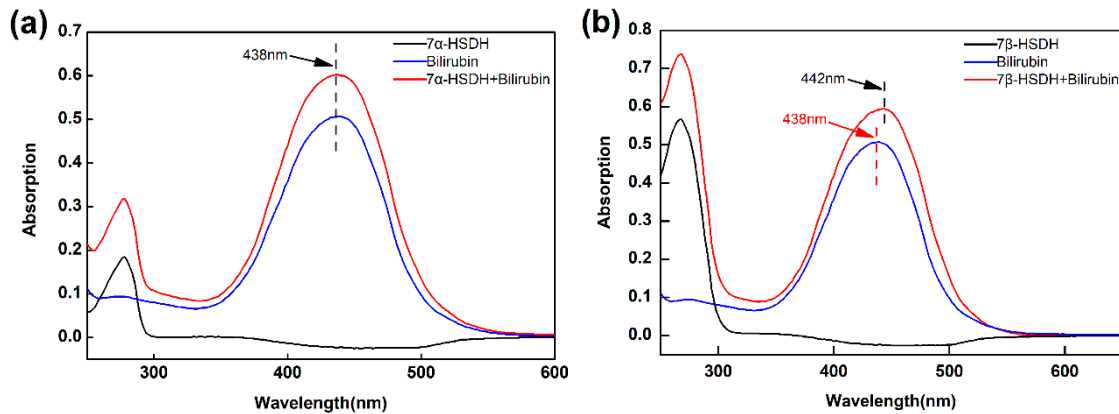
Figure 6. The analysis for combination of bilirubin to 7α- or 7β-HSDH by UV-Vis spectra. (**a**) For 7α-HSDH; (**b**) For 7β-HSDH. The PBS buffer (10mM, pH 7.4) was used as a background. 7α-HSDH+bilirubin and 7β-HSDH+bilirubin represented 7α-HSDH binding with 0.2 mM bilirubin and 7β-HSDH binding with 0.2 mM bilirubin, respectively.

After the molecular interaction, the fluorescence intensity of samples decreased and fluorescence quenching occurred. By studying this phenomenon, the binding mechanism of two molecules would be easily obtained. Quenching can be divided into two forms, dynamic or static. For dynamic quenching, a collision happened between the fluorophore and quencher. For static quenching, a ground state complex formed between the fluorophore and quencher [44].

So, the interactions of bilirubin to enzymes were investigated by florescence quenching from 350 nm to 600 nm, using 7α- and 7β-HSDH as the fluorophore and bilirubin as the quencher. The results were presented in Figure 7. Figure 7a showed the fluorescence spectra emission of 7α-HSDH in the presence of bilirubin at 25 °C. 7α-HSDH exhibited a broadband emission with a maximum at 448 nm when it was excited at 280 nm. According to literatures, the shift in position of emission maximum corresponded to the changes of the polarity around the chromospheres molecule [45,46]. The maximum emission wavelength of 7α-HSDH shifted from 448 to 511 nm, suggesting that the surroundings of the fluorophore are less polar when bilirubin interacts with the protein [47]. Figure 7b showed the fluorescence spectra emission of 7β-HSDH in the presence of bilirubin at 25 °C. Compared with 7α-HSDH, the fluorescence spectra emission of 7β-HSDH was more obvious after binding with bilirubin. The maximum emission of 7β-HSDH was at 440 nm when it was excited at 280 nm. The different results may be attributed to different compositions of tryptophan and tyrosine for 7α- and 7β-HSDH. The previous research had demonstrated that bilirubin was most possibly binding with arginine residue of human serum albumin. Bilirubin possessed an electron-rich surface that created van der Waals, stacking, and charge transfer interactions with tryptophan [43]. Bisphenols affected the activity of 11β-Hydroxysteroid dehydrogenase 2 by binding to the steroid-binding site and interacting with the catalytic residue tyrosine232 [48].
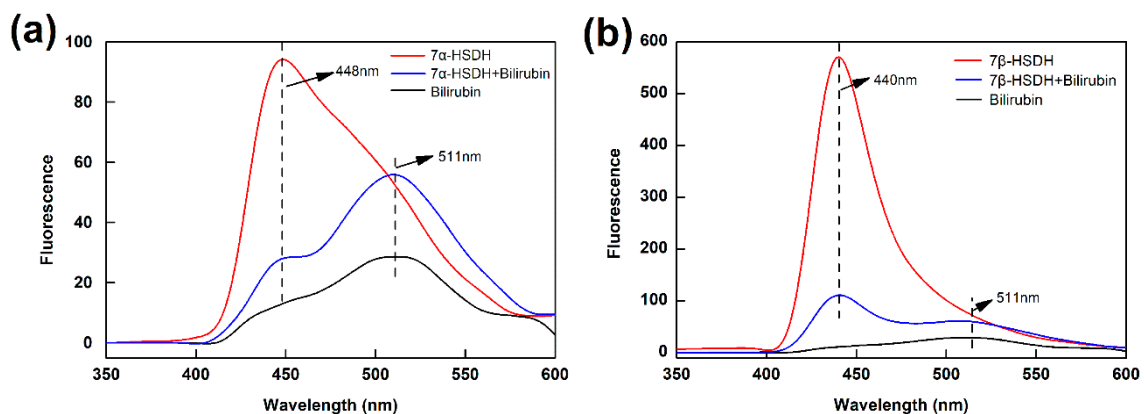
Figure 7. The analysis for combination of bilirubin to 7α- or 7β-HSDH by fluorescence spectra. The enzymes were excited at 280 nm. (**a**) For 7α-HSDH; (**b**) For 7β-HSDH. The PBS buffer (10mM, pH 7.4) was used as a background. 7α-HSDH+bilirubin and 7β-HSDH+bilirubin represented 7α-HSDH binding with 0.2 mM bilirubin and 7β-HSDH binding with 0.2 mM bilirubin, respectively.

CD spectrum is widely used to evaluate the secondary structure, folding, and binding properties of proteins since different structural elements have unique CD spectra at a particular wavelength [49]. So, the combinations of bilirubin to enzymes were analyzed by CD spectra from 250 nm to 550 nm. Figure 8 showed the typical induced CD spectra of bilirubin bound to 7α- or 7β-HSDH at molar ratios of 1 : 1. Bilirubin, 7α- and 7β-HSDH did not exhibit any dichroism. The solution of 7β-HSDH binding with 0.2 mM bilirubin exhibited similar CD spectra with 7α-HSDH binding with 0.2 mM bilirubin. 7α-HSDH induced a positive CD spectrum with a peak and a trough at 381 nm and 486 nm, respectively, and a cross-over at 415 nm. 7β-HSDH induces a positive bisignate CD spectrum with the peak, cross-over and trough at 329, 375 and 475 nm, respectively. Probably, after binding with bilirubin, the entropy of 7α- and 7β-HSDH were changed, which lead to the change of secondary structure. The changes reflected and recorded by CD spectrum.
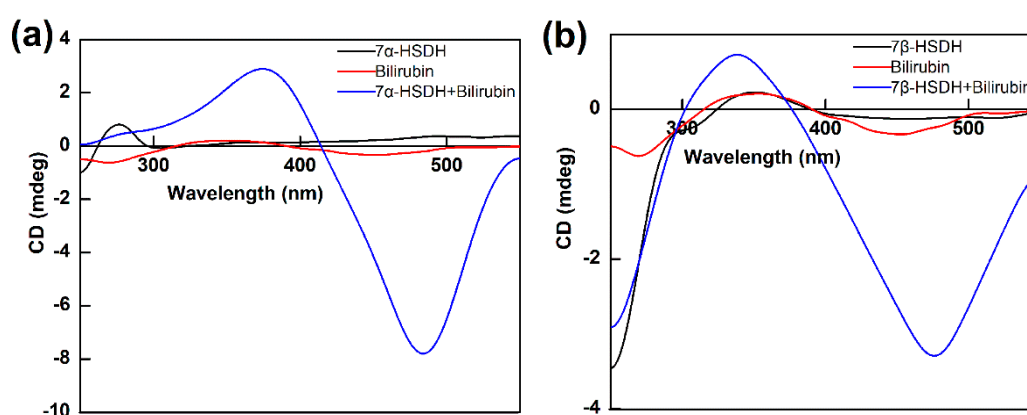

Figure 8. The analysis for combination of bilirubin to 7α- or 7β-HSDH by CD spectra. Bilirubin bound to 7α- or 7β-HSDH at molar ratios of 1 : 1. (**a**) For 7α-HSDH; (**b**) For 7β-HSDH. The PBS buffer (10mM, pH 7.4) was used as a background. 7α-HSDH+bilirubin and 7β-HSDH+bilirubin represented 7α-HSDH binding with 0.2 mM bilirubin and 7β-HSDH binding with 0.2 mM bilirubin, respectively.

The CD spectra of bilirubin bound to 7α- or 7β-HSDH with different proportions were shown in Figure 9. The molar ratios of 7α- or 7β-HSDH to bilirubin were 1 : 1, 1 : 3 and 1 : 5, which were stand for by black, red, and blue lines. The addition of bilirubin led to a gradual increase of the CD signal. Similar results were presented in groups both 7α-HSDH binding with bilirubin and 7β-HSDH binding with bilirubin. As Figure 9a, compared with 7α-HSDH/bilirubin = 1/1 molar ratio, the original value increase of 7α-HSDH/bilirubin = 1/5 reached 44% for positive component and 38% for negative component. As Figure 9b, compared with 7β-HSDH/bilirubin = 1/1 molar ratio, the original value increase of 7β-HSDH/bilirubin = 1/5 reached for 54% positive component and 46% for negative component, respectively. We assume bilirubin can bound to different sites of 7α- or 7β-HSDH. More than one bilirubin molecule combined with enzymes at the same time. With the increase of the binding amount of bilirubin, the structure changes of 7α- or 7β-HSDH may be more obvious.
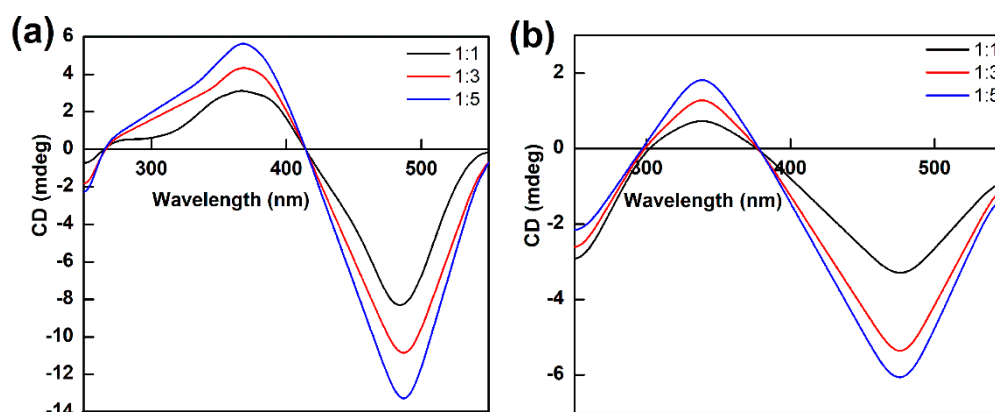
Figure 9. The CD spectrum of 7α- or 7β-HSDH binding with bilirubin under different proportions. The molar ratios of 7α- or 7β-HSDH to bilirubin were 1 : 1, 1 : 3 and 1 : 5. (**a**) For 7α-HSDH binding with bilirubin; (**b**) For 7β-HSDH binding with bilirubin. The PBS buffer (10mM, pH 7.4) was used as a background. The concentration of enzyme is 0.2mM.
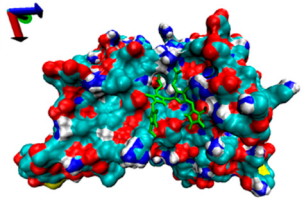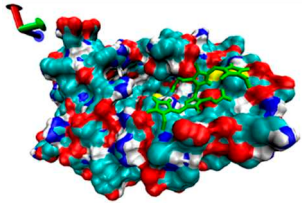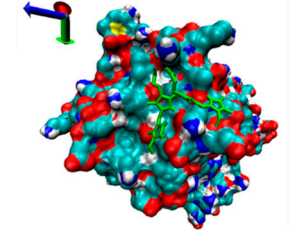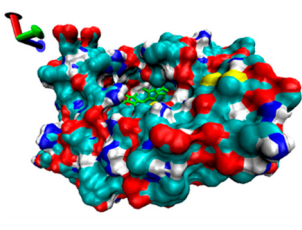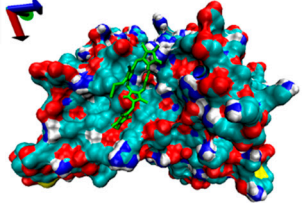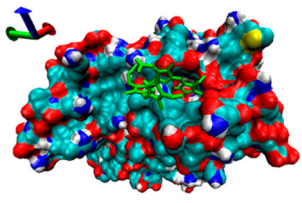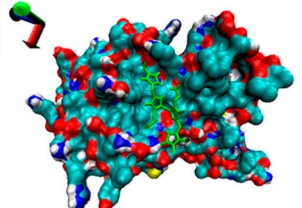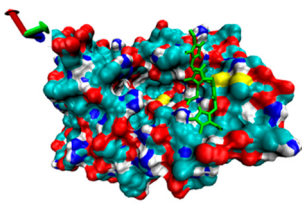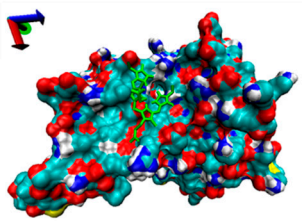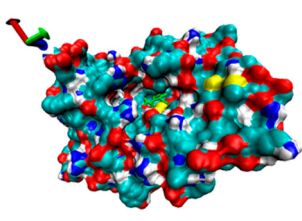
2.6. Exploration of inhibition mechanism

Molecular Docking is one computational simulation of a candidate ligand binding to a receptor, which is one of the most frequent used methods in structure-based binding of small molecule to functional protein. In order to further clarify the inhibition mechanisms of bilirubin on 7α- or 7β-HSDH, the random docking was conducted by AutoDock 4.2, and 10 candidate docking conformations were chosen for analysis as Table 3.

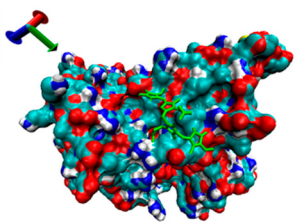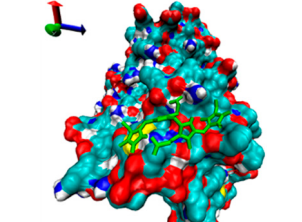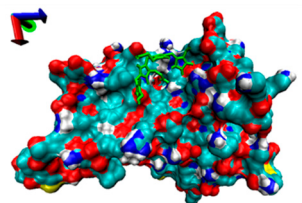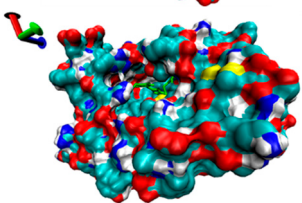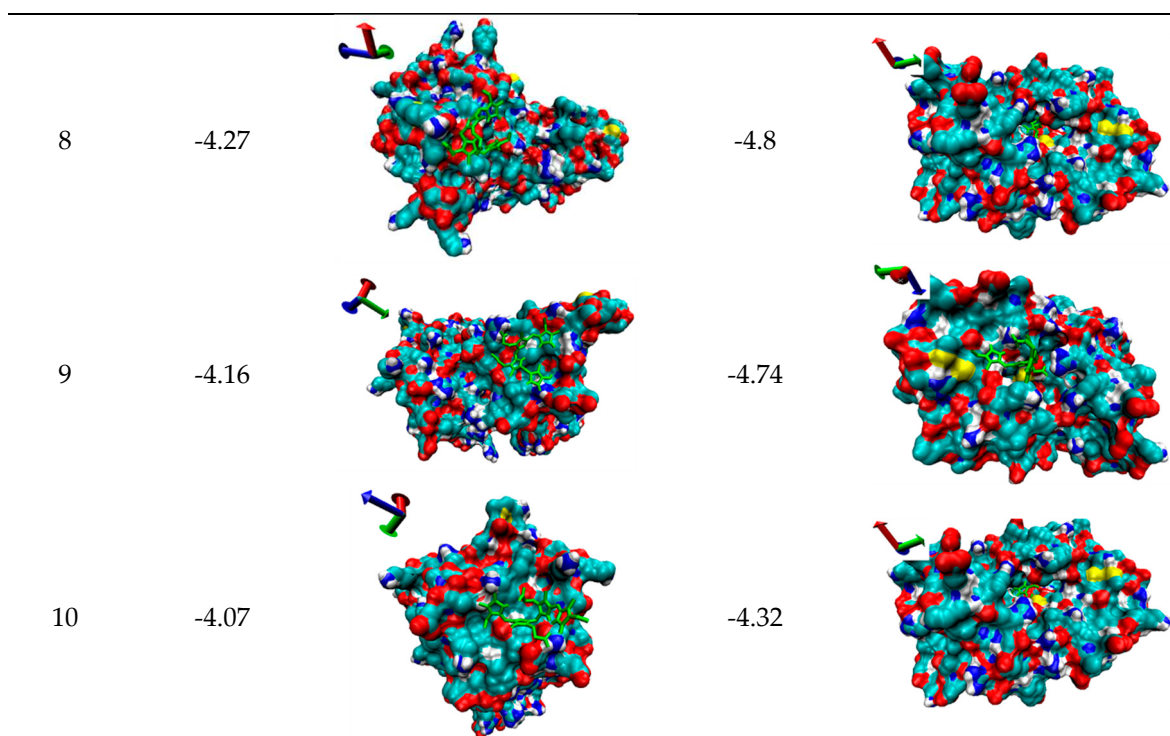The probably structures of 7α-HSDH after binding with bilirubin were shown in Table 3 according to binding energy. Structure 1 had the lowest energy value. The binding sites of bilirubin for structure 1, 3, 5 and 7 are in adjacent area. So this region is the most probably binding area of bilirubin and 7α-HSDH. From Figure S1, we can see the most probably binding site of bilirubin was close to NADP⁺, and bilirubin may be bound with Arg (16), Arg (20), Arg (194) and Glu (221) of 7α-HSDH. The previous study had demonstrated that bilirubin was also most possibly binding with arginine residue of human serum albumin [43]. Li et al. reported that triclosan, triflumizole and dichlone can bind to NAD⁺-binding site of human placental 3β-hydroxysteroid dehydrogenase [50]. According to reference [51], this region was exactly located at the cofactor-binding site. Three arginines at the position 16, 38 and 194 of 7α-HSDH form a positive environment surrounded the 2′-phosphate of adenine ribose of NADP⁺. Perhaps, the formation of hydrogen bonds were broken the transfer of H⁺ was hindered after the binding with bilirubin. It was no wonder that the activity of 7α-HSDH was inhibited. In summary, structure 1 was the most probable pose for the binding of bilirubin to 7α-HSDH. Refer to the kinetic constants (Table 2), after binding with bilirubin, the V_{max} of 7α-HSDH to NADP⁺ only had a minor change and the K_m of 7α-HSDH to NADP⁺ has a significantly increase. So it was determined that the inhibition of bilirubin to 7α-HSDH belong to competitive inhibition. This was consistent with the result of the molecular docking simulation.

The probably structures of 7β-HSDH after binding with bilirubin were also shown in Table 3 according to binding energy. Structure 1 had the lowest energy value. For 7β-HSDH, the binding sites of bilirubin are located at the channel entrance for structure 1, 3, 4 and 9. Five docking structures of 2, 5, 7, 8 and 10 reflect that bilirubin can enter the inner space of 7β-HSDH (as Table 3). Based on the analysis of optimum docking conformation, the most probably binding residues of bilirubin were Arg (40), Met (97) and Lys (107) of 7β-HSDH as Figure S2, which were located at the channel entrance for substrate and product. Access of substrate and product was restricted that may lead to the activity decrease of 7β-HSDH. Structure 1 was the most probable pose for the binding of bilirubin to 7β-HSDH. What's more, after binding with bilirubin, both the V_{max} and the K_m of 7β-HSDH to NADP⁺ decreased. So it was determined that the inhibition of bilirubin to 7β-HSDH belong to uncompetitive inhibition and the inhibition mechanism of bilirubin to 7β-HSDH was different from 7α-HSDH.

Table 3. 10 candidate docking results of 7α- or 7β-HSDH binding with bilirubin.

Number	7α-HSDH binding with bilirubin		7β-HSDH binding with bilirubin	
	Binding energy (kcal/mol)	Structures	Binding energy (kcal/mol)	Structures
1	-4.71		-5.79	
2	-4.67		-5.62	
3	-4.6		-5.39	
4	-4.55		-4.97	
5	-4.39		-4.91	
6	-4.35		-4.68	
7	-4.31		-4.83	

8	-4.27		-4.8
9	-4.16		-4.74
10	-4.07		-4.32

Molecular docking was performed on autodock 4.2 and the results were analyzed by VMD 1.8.3. The bilirubin molecule is labeled green. The docking results are ranked from small to large by the binding free energy and the axes are located in the upper left corner of each picture. Binding energy is include van der Waals force, Hydrogen bond, Desolvation energy and Electrostatic interaction.

3. Materials and Methods

3.1. Materials

7α-HSDH (EC 1.1.1.159) and 7β-HSDH (EC 1.1.1.201) were prepared by our laboratory. The amplified genes of two enzymes were cloned into the expression vector pGEX-6p-2, respectively. Recombinant plasmids were transformed into BL21 (DE3) and induced by 0.2 mM isopropyl β-D thiogalactoside (IPTG). After expression, target proteins were extracted by sonication. 7α-HSDH and 7β-HSDH were purified from bacterial lysates using GST affinity tag. You can refer to supplementary material to access the detailed preparation protocol of enzymes.

The bilirubin used in this study was purchased from Sigma-Aldrich (Product code: 14370), the purity of bilirubin is 95%. A BCA Protein Assay Reagent was product of Beyotime (P0010, Shanghai, China). The standards of TCDCA and TUDCA were purchased from the National Institutes for Food and Drug Control (Beijing, China). Sodium taurine-7-ketolithocholic acid (T-7-KLCA) was synthesized by our laboratory. The reaction cofactors, NADP-Na$_2$ and NADPH-Na$_4$ (Purity≥97%) were acquired from Roche (Switzerland). All the other chemicals used in this study were of analytical grade and used without further purification. Double-distilled water was used in all experiments.

3.2. Properties of 7α- and 7β-HSDH

After expression and purification, 7α- and 7β-HSDH were monitored by sodium dodecyl sulphate polyacrylamide gel electrophoresis (SDS-PAGE). After the separation Gel (12 %) solidified, 5 % spacer gel was prepared and the appropriate comb was selected. Transfer protein sample (10 μL) to fresh tube, add 2 μL of 6 × SDS loading buffer, and vortex briefly and heat for 5 min at 100 °C. Run the gel for the appropriate length of time and stain with Coomassie blue for about 30 min. Decolorize with destaining solution until the bands were clear. Protein concentration was measured by BCA protein assay using bovine serum albumin as a standard. Purified protein was stored at -80 °C with 20% glycerol for further use. The properties of 7α- and 7β-HSDH were estimated by peptide

calculator (Qiangyao, Shanghai) according to references [52], such as molecular weight, isoelectric point, charge condition, average hydrophilicity and ratio of hydrophilic residues.

3.3. Enzymatic activity and kinetic characterization

The activities of 7α- and 7β-HSDH were assayed according to references [16,17], with slight modifications. For the determination of 7α-HSDH activity, the enzyme assay mixture in a total volume of 1 mL was: 2 mM TCDCA in 50 mM Tris-HCl, pH 8.5, and 0.2 mM NADP$^+$. Determination of 7β-HSDH activity was performed in a total volume of 1 mL assay mixture containing: 2 mM TUDCA in 50 mM Tris–HCl, pH 8.5, and 0.2 mM NADP$^+$. The amount of NADPH was proportional to the ultraviolet absorption at 340 nm. So change of absorbance at 340 nm was recorded by a spectrophotometer (UV 1800, Shimadzu, Japan) to evaluate enzymes activity. One unit of enzyme activity was defined as the amount of enzyme needed to convert 1 μM substrate (TCDCA/TUDCA) within 1 min at 25 °C in a buffer solution containing 50 mM Tris-HCl (pH 8.5).

The kinetic studies of 7α-HSDH and 7β-HSDH were performed by measuring the reduction of NADP$^+$ at 340 nm using UV-vis spectrophotometer (UV 1800, Shimadzu, Japan) according to the previously reported methods [16,17]. Kinetic parameters were calculated by the Michaelis–Menten equation as follows: $v = V_{max} \cdot [S] / (K_m + [S])$, where, $[S]$ is the substrate concentration. v and V_{max} represent the initial and maximum rate of reaction, respectively. K_m is the Michaelis constant.

3.4. Enzymatic reaction

The reaction was carried out on the condition of 25 °C, pH 8.5 Tris–HCl (50 mM), using TCDCA (8 mM) as substrate. The final concentration of both 7α-HSDH and 7β-HSDH were 0.5 mg/L, and the concentration of NADP$^+$ was 2 mM. The reaction was continued for 4 hours with the catalysis of free 7α- and 7β-HSDH. All tests were performed in triplicate and expressed as the means ± SD (n = 3). TCDCA conversion and TUDCA yield were analysed by HPLC-ELSD and evaluated as follows:

$$\text{TCDCA Conversion} = \frac{\text{Total amount of TCDCA added (g) - Total amount of TCDCA remaining (g)}}{\text{Total amount of TCDCA added (g)}} \times 100\% \tag{1}$$

$$\text{TUDCA Yield} = \frac{\text{Total amount of TUDCA generated (g)}}{\text{Total amount of TCDCA added (g)}} \times 100\% \tag{2}$$

3.5. The effect of bilirubin on enzyme activity and TCDCA transformation

The effect of bilirubin on the activity of enzymes and TCDCA transformation were studied according to the following methods. For enzyme activity, bilirubin added to the solution of TCDCA or TUDCA at 25 °C (50 mM Tris–HCl, pH 8.5), and the final concentration of bilirubin varied from 0 to 1.0 μM. Enzyme activity in the absence of bilirubin set to 100% and the relative activity in the presence of bilirubin can be obtained. Furthermore, the effects of bilirubin (0.2 mM) on the kinetic parameters of 7α- and 7β-HSDH were investigated. The analyses of enzyme activity and kinetics were according to the protocol 3.3. For enzymatic reaction, the effect of bilirubin on coupling-reaction was determined by testing various bilirubin concentrations ranging from 0 to 0.8 mM with a gradient per 0.2 mM, in 50 mM Tris–HCl buffer (pH 8.5). Furthermore, the composition of products was analyzed by HPLC-ELSD. TCDCA conversion and TUDCA yield calculated based on the equations of protocol 3.4. Other reaction conditions were consistent. All tests were performed in triplicate.

3.6. The combination analysis of bilirubin and enzymes

3.6.1. UV–Vis spectrum

The binding of bilirubin and enzymes was analysed by UV–Vis spectrum. The enzyme solution (7α-HSDH or 7β-HSDH) was dilute to a concentration 1.2×10^{-5} moL/L. Bilirubin solution with the same concentration was used for analysis. Besides, a mixture solution was obtained by mixing the equivalent volume of bilirubin stock solution and the equivalent volume of enzyme stock solution at

a phosphate buffered saline (PBS) of pH = 7.4. The samples were scanned against PBS buffer (10mM, pH 7.4) background by a wave number ranging from 250 nm to 600 nm with a 1 cm path length.

3.6.2. Fluorescence spectrum

The binding of bilirubin and enzymes was analysed by Fluorescence spectrum. Fluorescence measurements were performed on a spectrofluorimeter (LS55, Perkinelmer, USA) equipped with thermostatisation systems and a temperature controller, using 5 nm excitation and 5 nm emission slit widths. The three samples (enzyme solution, bilirubin solution and the mixture of two solutions with molar ratio 1 : 1 for enzyme and bilirubin) were excited at 280 nm and scanned in the range of 350–600 nm with 100 nm min^{-1} scanning speed. The PBS buffer (10mM, pH 7.4) was used as a background.

3.6.3. CD spectrum

The binding of bilirubin and enzymes was analysed by CD spectrum. The CD spectra of three solutions (enzyme solution, bilirubin solution, the mixture solutions of enzyme and bilirubin with molar ratio 1 : 1, 1 : 3 and 1 : 5) were recorded on a CD spectrometer (MOS450, Bio-Logic, France) under nitrogen atmosphere using a quartz cell with a path length of 1 cm. All the experiments were run at 25 °C. The CD spectra were recorded at 250–550 nm wavelength region as an average of three scans measured with a 1 nm bandwidth, a 1 s response and 100 nm min^{-1} scanning speed. All of the CD spectra of samples were baseline PBS buffer (10mM, pH 7.4) by using a spectrum of the solvent obtained under the same experimental conditions.

3.7. High performance liquid chromatography (HPLC)

HPLC analysis was performed using Agilent 1260 Infinity (Agilent Technologies, USA) with evaporative light-scattering detector, and chromatographic separations were conducted on a Welch ultimate XB-C18 column (4.6 × 250 mm, 5 μm). The analysis was carried out in nitrogen environment and the speed of nitrogen was 1.2 L·min^{-1} and the temperature of ELSD detector set to 80 °C. Methanol was used as solvent and the injection volume set to 10 μL. The mobile phase consisted by two solvents, solution A: 100% acetonitrile; solution B: 30 mM aqueous ammonium acetate solution (pH 4.5). The analysis was conducted with 42% solution A and 58% solution B. Furthermore, the analysis time was for 10 min and a constant flow rate of 1.0 mL· min^{-1} was adopted.

3.8. Molecular docking of bilirubin and enzymes

The goal of bilirubin-protein docking is to predict the predominant binding modes of bilirubin with 7α-HSDH or 7β-HSDH, which have known three-dimensional structure. Furthermore, we can analyze the inhibition mechanisms of bilirubin to 7α-HSDH or 7β-HSDH based on the dockings. The 3D crystal structure of 7α-HSDH (PDB code: 5EPO) and 7β-HSDH (PDB code: 5GT9) obtained from the Protein Data Bank [51,53]. The ionizable residues were set to protonation states (pH 7.4). In this state, all His, Arg and Lys were protonated while Asp and Glu were deprotonated. The AutoDock 4.2 plugin was used for all dockings in this study. The docking parameters for AutoDock 4.2 were kept to their default values. The docking results were ranked by the binding free energy, 10 candidate dockings were selected for analysis. The optimum docking conformation was chosen based on the lowest binding free energy and the most cluster members. Visual Molecular Dynamics 1.8.3 (VMD 1.8.3) was used to illustrate the binding results.

4. Conclusions

In conclusion, we systematically investigated the impact of bilirubin on 7α- and 7β-HSDH, including the effect of bilirubin on enzymes activities and enzymatic reaction. After binding with bilirubin, the K_m of 7α-HSDH for TCDCA rose from 0.24 mM to 0.63 mM, the K_m of 7β-HSDH for TUDCA changed from 1.14 mM to 1.87 mM. The affinity of 7α- and 7β-HSDH to substrate decreased after binding with bilirubin. With the increase of bilirubin, both TCDCA conversion and TUDCA yield were gradually decreased. As the concentration of bilirubin was 0.8 mM in reaction buffer,

TCDCA conversion remained 15% and TUDCA yield was only 5%. The binding of bilirubin to 7α- or 7β-HSDH will lead to the significant changes of enzymes spectrum, such as UV–Vis spectrum, Fluorescence spectrum and CD spectrum. The enzymatic activity loss and response of spectrum may be related to the structure changes of enzymes after binding with bilirubin. Molecular Docking was conducted to explore the possible inhibition mechanism of bilirubin to enzymes. The most probably binding site of bilirubin to 7α-HSDH was close to NADP$^+$, and the most probably binding residues of bilirubin to 7β-HSDH were located at the channel entrance for substrate and product. Refer to the kinetic parameters, we conclude that the inhibition of bilirubin to 7α-HSDH belongs to a competitive inhibition and the inhibition of bilirubin to 7β-HSDH belongs to an uncompetitive inhibition. Further research about the effects of bilirubin on other hydroxysteroid dehydrogenases will be gradual promoted.

References

1. Wahlström, A.; Sayin, Sama I.; Marschall, H.-U.; Bäckhed, F. Intestinal Crosstalk between Bile Acids and Microbiota and Its Impact on Host Metabolism. Cell Metab. **2016**, *24*, 41-50. https://doi.org/10.1016/j.cmet.2016.05.005.
2. Vallim, T.Q.D.; Tarling, E.J.; Edwards, P.A. Pleiotropic Roles of Bile Acids in Metabolism. Cell Metab. **2013**, *17*, 657-669. https://doi.org/10.1016/j.cmet.2013.03.013.
3. Alpini, G.; Baiocchi, L.; Glaser, S.; Ueno, Y.; Marzioni, M.; Francis, H.; Phinizy, J.L.; Angelico, M.; LeSage, G. Ursodeoxycholate and tauroursodeoxycholate inhibit cholangiocyte growth and secretion of BDL rats through activation of PKC alpha. Hepatology **2002**, *35*, 1041-1052. https://doi.org/10.1053/jhep.2002.32712.
4. Harms, M.H.; van Buuren, H.R.; Corpechot, C.; Thorburn, D.; Janssen, H.L.A.; Lindor, K.D.; Hirschfield, G.M.; Parés, A.; Floreani, A.; Mayo, M.J.; et al. Ursodeoxycholic acid therapy and liver transplant-free survival in patients with primary biliary cholangitis. J. Hepatol. **2019**, *71*, 357-365. https://doi.org/10.1016/j.jhep.2019.04.001.
5. Wu, P.; Zhao, J.; Guo, Y.; Yu, Y.; Wu, X.; Xiao, H. Ursodeoxycholic acid alleviates nonalcoholic fatty liver disease by inhibiting apoptosis and improving autophagy *via* activating AMPK. Biochem. Biophys. Res. Commun. **2020**, *529*, 834-838. https://doi.org/10.1016/j.bbrc.2020.05.128.
6. Fernandez-Sanchez, L.; Lax, P.; Noailles, A.; Angulo, A.; Maneu, V.; Cuenca, N. Natural Compounds from Saffron and Bear Bile Prevent Vision Loss and Retinal Degeneration. Molecules **2015**, *20*, 13875-13893. https://doi.org/10.3390/molecules200813875.
7. Hu, J.; Xu, M.; Yuan, J.; Li, B.; Entenman, S.; Yu, H.; Zheng, Q.Y. Tauroursodeoxycholic Acid Prevents Hearing Loss and Hair Cell Death in Cdh23erl/Erl Mice. Neuroscience **2016**, *316*, 311-320. https://doi.org/10.1016/j.neuroscience.2015.12.050.
8. Qi, H.; Shen, D.; Jiang, C.; Wang, H.; Chang, M. Ursodeoxycholic acid protects dopaminergic neurons from oxidative stress via regulating mitochondrial function, autophagy, and apoptosis in MPTP/MPP+-induced Parkinson's disease. Neurosci. Lett. **2021**, *741*, 135493. https://doi.org/10.1016/j.neulet.2020.135493.
9. Rosa, A.I.; Duarte-Silva, S.; Silva-Fernandes, A.; Nunes, M.J.; Carvalho, A.N.; Rodrigues, E.; Gama, M.J.; Rodrigues, C.M.P.; Maciel, P.; Castro-Caldas, M. Tauroursodeoxycholic Acid Improves Motor Symptoms

in a Mouse Model of Parkinson's Disease. Mol. Neurobiol. **2018**, *55*, 9139-9155. https://doi.org/10.1007/s12035-018-1062-4.

10. Cho, J.G.; Lee, J.H.; Hong, S.H.; Lee, H.N.; Kim, C.M.; Kim, S.Y.; Yoon, K.J.; Oh, B.J.; Kim, J.H.; Jung, S.Y.; et al. Tauroursodeoxycholic Acid, a Bile Acid, Promotes Blood Vessel Repair by Recruiting Vasculogenic Progenitor Cells. Stem Cells **2015**, *33*, 792-805. https://doi.org/10.1002/stem.1901.

11. Guo, Q.; Shi, Q.; Li, H.; Liu, J.; Wu, S.; Sun, H.; Zhou, B. Glycolipid Metabolism Disorder in the Liver of Obese Mice Is Improved by TUDCA *via* the Restoration of Defective Hepatic Autophagy. Int. J. Endocrinol. **2015**, *2015*, 11. https://doi.org/10.1155/2015/687938.

12. Nabil, T.M.; Khalil, A.H.; Gamal, K. Effect of oral ursodeoxycholic acid on cholelithiasis following laparoscopic sleeve gastrectomy for morbid obesity. Surg. Obes. Relat. Dis. **2019**, *15*, 827-831. https://doi.org/10.1016/j.soard.2019.03.028.

13. Lee, Y.Y.; Hong, S.H.; Lee, Y.J.; Chung, S.S.; Jung, H.S.; Park, S.G.; Park, K.S. Tauroursodeoxycholate (TUDCA), chemical chaperone, enhances function of islets by reducing ER stress. Biochem. Biophys. Res. Commun. **2010**, *397*, 735-739. https://doi.org/10.1016/j.bbrc.2010.06.022.

14. Brevini, T.; Maes, M.; Webb, G.J.; John, B.V.; Fuchs, C.D.; Buescher, G.; Wang, L.; Griffiths, C.; Brown, M.L.; Scott, W.E.; et al. FXR inhibition may protect from SARS-CoV-2 infection by reducing ACE2. Nature **2022**. https://doi.org/10.1038/s41586-022-05594-0.

15. Zheng, M.M.; Wang, R.F.; Li, C.X.; Xu, J.H. Two-step enzymatic synthesis of ursodeoxycholic acid with a new 7 beta-hydroxysteroid dehydrogenase from *Ruminococcus torques*. Process Biochem. **2015**, *50*, 598-604. https://doi.org/10.1016/j.procbio.2014.12.026.

16. Ji, Q.Z.; Tan, J.; Zhu, L.C.; Lou, D.S.; Wang, B.C. Preparing tauroursodeoxycholic acid (TUDCA) using a double-enzyme-coupled system. Biochem. Eng. J. **2016**, *105*, 1-9. https://doi.org/10.1016/j.bej.2015.08.005.

17. Ferrandi, E.E.; Bertolesi, G.M.; Polentini, F.; Negri, A.; Riva, S.; Monti, D. In search of sustainable chemical processes: cloning, recombinant expression, and functional characterization of the 7 alpha- and 7 beta-hydroxysteroid dehydrogenases from *Clostridium absonum*. Appl. Microbiol. Biotechnol. **2012**, *95*, 1221-1233. https://doi.org/10.1007/s00253-011-3798-x.

18. Bennett, M.J.; McKnight, S.L.; Coleman, J.P. Cloning and characterization of the NAD-dependent 7 alpha-hydroxysteroid dehydrogenase from *Bacteroides fragilis*. Curr. Microbiol. **2003**, *47*, 475-484. https://doi.org/10.1007/s00284-003-4079-4.

19. Pedrini, P.; Andreotti, E.; Guerrini, A.; Dean, M.; Fantin, G.; Giovannini, P.P. *Xanthomonas maltophilia* CBS 897.97 as a source of new 7 beta- and 7 alpha-hydroxysteroid dehydrogenases and cholylglycine hydrolase: Improved biotransformations of bile acids. Steroids **2006**, *71*, 189-198. https://doi.org/10.1016/j.steroids.2005.10.002.

20. Huang, B.; Yang, K.; Amanze, C.; Yan, Z.; Zhou, H.; Liu, X.; Qiu, G.; Zeng, W. Sequence and structure-guided discovery of a novel NADH-dependent 7β-hydroxysteroid dehydrogenase for efficient biosynthesis of ursodeoxycholic acid. Bioorg. Chem. **2023**, *131*, 106340. https://doi.org/10.1016/j.bioorg.2022.106340.

21. Ji, S.; Pan, Y.; Zhu, L.; Tan, J.; Tang, S.; Yang, Q.; Zhang, Z.; Lou, D.; Wang, B. A novel 7α-hydroxysteroid dehydrogenase: Magnesium ion significantly enhances its activity and thermostability. Int. J. Biol. Macromol. **2021**, *177*, 111-118. https://doi.org/10.1016/j.ijbiomac.2021.02.082.

22. Ji, Q.; Wang, B.; Li, C.; Hao, J.; Feng, W. Co-immobilised 7α- and 7β-HSDH as recyclable biocatalyst: high-performance production of TUDCA from waste chicken bile. RSC Advances **2018**, *8*, 34192-34201. https://doi.org/10.1039/c8ra06798h.

23. Stocker, R.; Yamamoto, Y.; Mcdonagh, A.; Glazer, A.; Ames, B.J.S. Bilirubin is an antioxidant of possible physiological importance. Science **1987**, *235*, 1043-1046.

24. Baraano, D.E.; Rao, M.; Ferris, C.D.; Snyder, S.H. Biliverdin reductase: a major physiologic cytoprotectant. Proc. Natl. Acad. Sci. USA. **2002**. 99, 16093–16098. https://doi.org/10.1073/pnas.252626999.

25. Vitek, L.; Hinds, T.D.; Stec, D.E.; Tiribelli, C. The physiology of bilirubin: health and disease equilibrium. Trends Mol. Med. **2023**, *29*, 315-328. https://doi.org/10.1016/j.molmed.2023.01.007.

26. Liu, H.W.; Gong, L.N.; Lai, K.; Yu, X.F.; Liu, Z.Q.; Li, M.X.; Yin, X.L.; Liang, M.; Shi, H.S.; Jiang, L.H.; et al. Bilirubin gates the TRPM2 channel as a direct agonist to exacerbate ischemic brain damage. Neuron **2023**. https://doi.org/10.1016/j.neuron.2023.02.022.

27. Zhou, S.; Wei, Y. Kaleidoscope megamolecules synthesis and application using self-assembly technology. Biotechnol. Adv. **2023**, 108147. https://doi.org/10.1016/j.biotechadv.2023.108147.

28. Wang, Z.; Guo, Y.; Xianyu, Y. Applications of self-assembly strategies in immunoassays: A review. Coord. Chem. Rev. **2023**, *478*, 214974. https://doi.org/10.1016/j.ccr.2022.214974.

29. Afzal, M.I.; Shahid, S.; Mansoor, S.; Javed, M.; Iqbal, S.; Hakami, O.; Yousef, E.S.; Al-Fawzan, F.F.; Elkaeed, E.B.; Pashameah, R.A.; et al. Fabrication of a Ternary Nanocomposite g-C3N4/Cu@CdS with Superior Charge Separation for Removal of Organic Pollutants and Bacterial Disinfection from Wastewater under Sunlight Illumination. Toxics **2022**, *10*, 657. https://doi.org/10.3390/toxics10110657

30. Fazal, T.; Iqbal, S.; Shah, M.; Ismail, B.; Shaheen, N.; Alharthi, A.I.; Awwad, N.S.; Ibrahium, H.A. Correlation between structural, morphological and optical properties of Bi$_2$S$_3$ thin films deposited by various aqueous and non-aqueous chemical bath deposition methods. Results in Physics **2022**, *40*, 105817. https://doi.org/10.1016/j.rinp.2022.105817.

31. Girelli, A.M.; Chiappini, V. Renewable, sustainable, and natural lignocellulosic carriers for lipase immobilization: A review. J. Biotechnol. **2023**, *365*, 29-47. https://doi.org/10.1016/j.jbiotec.2023.02.003.

32. Zdarta, J.; Kołodziejczak-Radzimska, A.; Bachosz, K.; Rybarczyk, A.; Bilal, M.; Iqbal, H.M.N.; Buszewski, B.; Jesionowski, T. Nanostructured supports for multienzyme co-immobilization for biotechnological applications: Achievements, challenges and prospects. Adv. Colloid Interface Sci. **2023**, 102889. https://doi.org/10.1016/j.cis.2023.102889.

33. Odell, G.B. Studies in kernicterus. I. the protein binding of bilirubin, J. Clin. Invest. 1959, 38, 823-833..

34. Hulzebos, C.V.; Dijk, P.H. Bilirubin–albumin binding, bilirubin/albumin ratios, and free bilirubin levels: Where do we stand? Semin. Perinatol. **2014**, *38*, 412-421. https://doi.org/10.1053/j.semperi.2014.08.004.

35. Vítek, L.; Tiribelli, C. Bilirubin: The yellow hormone? J. Hepatol. **2021**, *75*, 1485-1490. https://doi.org/10.1016/j.jhep.2021.06.010.

36. Morioka, I.; Iwatani, S.; Koda, T.; Iijima, K.; Nakamura, H. Disorders of bilirubin binding to albumin and bilirubin-induced neurologic dysfunction. Semin. Fetal Neonat. M. **2015**, *20*, 31-36. https://doi.org/10.1016/j.siny.2014.11.001.

37. Amin, S.B. Bilirubin Binding Capacity in the Preterm Neonate. Clin. Perinatol. **2016**, *43*, 241-257. https://doi.org/10.1016/j.clp.2016.01.003.

38. Arriaga, S.M.; Basiglio, C.L.; Mottino, A.D.; Almará, A.M. Unconjugated bilirubin inhibits C1 esterase activity. Clin. Biochem. **2009**, *42*, 919-921. https://doi.org/10.1016/j.clinbiochem.2008.12.015.

39. Nagarajan, U.; Gladstone Christopher, J.; Jonnalagadda, R.R.; Chandrasekaran, B.; Balachandran, U.N. Studies on the chemico-biological characteristics of bilirubin binding with collagen. Mat. Sci. Eng.: C **2013**, *33*, 4965-4971. https://doi.org/10.1016/j.msec.2013.08.021.

40. Gligorijević, N.; Minić, S.; Robajac, D.; Nikolić, M.; Ćirković Veličković, T.; Nedić, O. Characterisation and the effects of bilirubin binding to human fibrinogen. Int. J. Biol. Macromol. **2019**, *128*, 74-79. https://doi.org/10.1016/j.ijbiomac.2019.01.124.

41. Michelin, M.; Ximenes, E.; M. Polizeli, M.d.L.T.; Ladisch, M.R. Inhibition of enzyme hydrolysis of cellulose by phenols from hydrothermally pretreated sugarcane straw. Enzyme Microb. Technol. **2023**, *166*, 110227. https://doi.org/10.1016/j.enzmictec.2023.110227.

42. Baksi, S.; Sarkar, U.; Villa, R.; Basu, D.; Sengupta, D. Conversion of biomass to biofuels through sugar platform: A review of enzymatic hydrolysis highlighting the trade-off between product and substrate inhibitions. Sustain. Energy Techn. **2023**, *55*, 102963. https://doi.org/10.1016/j.seta.2022.102963.

43. Orlov, S.; Goncharova, I.; Urbanova, M. Circular dichroism study of the interaction between mutagens and bilirubin bound to different binding sites of serum albumins. Spectrochim. Acta. A. **2014**, *126*, 68-75. https://doi.org/10.1016/j.saa.2014.01.139.

44. Beatriz; Rodríguez; Galdón; Carmen; Pinto; Corraliza; Juan; J.; Cestero; C.J. Spectroscopic study of the interaction between lycopene and bovine serum albumin. Luminescence 2013, 28, 765-770. https://doi.org/10.1002/bio.2434.

45. Ding, F.; Huang, J.; Lin, J.J.D.; Pigments. A study of the binding of C.I.Mordant Red 3 with bovine serum albumin using fluorescence spectroscopy. Dyes Pigments **2009**,1, 82. https://doi.org/10.1016/j.dyepig.2008.11.003.

46. Yuan, T.; Weljie, A.M.; Vogel, H.J. Tryptophan Fluorescence Quenching by Methionine and Selenomethionine Residues of Calmodulin: Orientation of Peptide and Protein Binding. Biochemistry (Mosc). **1998**, *37*, 3187-3195. https://doi.org/10.1021/bi9716579.

47. Guo, Y.; Yue, Q.; Gao, B.; Zhong, Q.J.J.o.L. Spectroscopic studies on the interaction between disperse blue SBL and bovine serum albumin. J. Lumin. **2010**, *130*, 1384-1389. https://doi.org/10.1016/j.jlumin.2010.02.051.

48. Zhang, B.; Wang, S.; Tang, Y.; Hu, Z.; Shi, L.; Lu, J.; Li, H.; Wang, Y.; Zhu, Y.; Lin, H.; et al. Direct inhibition of bisphenols on human and rat 11β-hydroxysteroid dehydrogenase 2: Structure-activity relationship and docking analysis. Ecotoxicol. Environ. Saf. **2023**, *254*, 114715. https://doi.org/10.1016/j.ecoenv.2023.114715.

49. Greenfield, N.J. Using circular dichroism spectra to estimate protein secondary structure. Nat. Protoc. **2006**, *1*, 2876-2890. https://doi.org/10.1038/nprot.2006.202.

50. Li, J.; Tian, F.; Tang, Y.; Shi, L.; Wang, S.; Hu, Z.; Zhu, Y.; Wang, Y.; Li, H.; Ge, R.S.; et al. Inhibition of human and rat placental 3β-hydroxysteroid dehydrogenase/Δ5,4-isomerase activities by insecticides and fungicides: Mode action by docking analysis. Chem. Biol. Interact. **2023**, *369*, 110292. https://doi.org/10.1016/j.cbi.2022.110292.

51. Lou, D.; Wang, B.; Tan, J.; Zhu, L.; Cen, X.; Ji, Q.; Wang, Y. The three-dimensional structure of *Clostridium absonum* 7α-hydroxysteroid dehydrogenase: new insights into the conserved arginines for NADP(H) recognition. Sci. Rep. **2016**, *6*, 22885. https://doi.org/10.1038/srep22885.

52. Lear, S.; Cobb, S.L. Pep-Calc.com: a set of web utilities for the calculation of peptide and peptoid properties and automatic mass spectral peak assignment. J. Comput. Aid. Mol. Des. **2016**, *30*, 271-277. https://doi.org/10.1007/s10822-016-9902-7.

53. Wang, R.; Wu, J.; Jin, D.K.; Chen, Y.; Lv, Z.; Chen, Q.; Miao, Q.; Huo, X.; Wang, F. Structure of NADP(+)-bound 7 beta-hydroxysteroid dehydrogenase reveals two cofactor-binding modes. Acta Cryst. **2017** *F73*, 246-252. https://doi.org/10.1107/S2053230X17004460.